Journal of Hazardous Materials 459 (2023) 132213

Contents lists available at ScienceDirect

Journal of Hazardous Materials

journal homepage: www.elsevier.com/locate/jhazmat

Fate of Cd during mineral transformation by sulfate-reducing bacteria in clay-size fractions from soils with high geochemical background

Xing Yan [a,1], Dong-Xing Guan [b,1], Jie Li [c], Yinxian Song [d], Hua Tao [e], Xianming Zhang [a], Ming Ma [c], Junfeng Ji [f], Wancang Zhao [a,*]

[a] Chongqing Key Laboratory of Karst Environment, School of Geographical Sciences, Southwest University, Chongqing 400715, PR China
[b] Zhejiang Provincial Key Laboratory of Agricultural Resources and Environment, Institute of Soil and Water Resources and Environmental Science, College of Environmental and Resource Sciences, Zhejiang University, Hangzhou 310058, PR China
[c] Center of Molecular Ecophysiology (CMEP), College of Resources and Environment, Southwest University, Chongqing 400715, PR China
[d] Department of Geosciences, Faculty of Land Resource Engineering, Kunming University of Science and Technology, Kunming 650093, Yunnan Province, PR China
[e] Chongqing Geological and Mineral Resource Exploration and Development Bureau 607 Geological Team, Chongqing 401120, PR China
[f] Key Laboratory of Surficial Geochemistry, Ministry of Education, School of Earth Sciences and Engineering, Nanjing University, Nanjing 210093, PR China

HIGHLIGHTS

- Clay-size fractions were extracted from soils with high Cd background for bacteria inoculation.
- Clay-size fractions were the primary reservoir (23–65%) for Cd in soil.
- Sulfate-reducing bacteria (SRB) promoted Cd redistribution and immobilization in clay.
- SRB facilitated the mineral conversion of iron oxides and the immobilization of Cd.

GRAPHICAL ABSTRACT

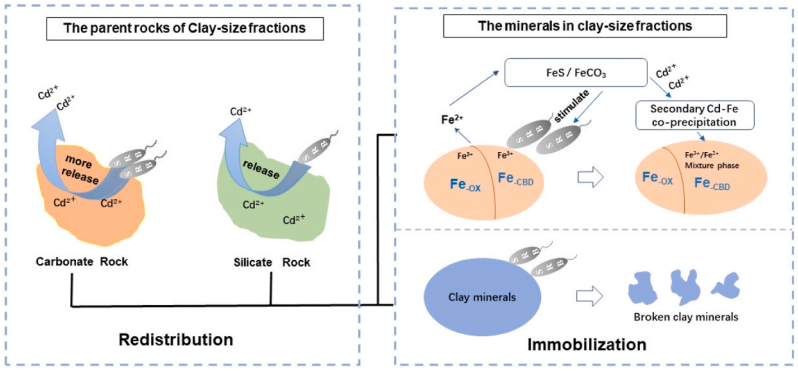

ARTICLE INFO

Editor: Jörg Rinklebe

Keywords:
Sulfate-reducing bacteria (SRB)
Clay-size fractions
Stratigraphic successions
Iron bearing minerals
Cd immobilization

ABSTRACT

Sulfate-reducing bacteria (SRB) can immobilize heavy metals in soils through biomineralization, and the parent rock and minerals in the soil are critical to the immobilization efficiency of SRB. To date, there is little knowledge about the fate of Cd associated with the parent rocks and minerals of soil during Cd immobilized by SRB. In this study, we created a model system using clay-size fraction of soil and SRB to explore the role of SRB in immobilizing Cd in soils from stratigraphic successions with high geochemical background. In the system, clay-size fractions (particle size < 2 μm) with concentration of Cd (0.24–2.84 mg/kg) were extracted from soils for bacteria inoculation. After SRB reaction for 10 days, the Cd fraction tended to transform into iron-manganese bound. Further, two clay-size fractions, i.e., the non-crystalline iron oxide (Fe_{-OX}) and the crystalline iron oxide (Fe_{-CBD}), were separated by extraction. The reaction of SRB with them verified the transformation of

* Corresponding author.
E-mail addresses: geodoer@swu.edu.cn, zhwc321@163.com (W. Zhao).
[1] These authors contributed as co-first authors in this paper.

https://doi.org/10.1016/j.jhazmat.2023.132213
Received 25 April 2023; Received in revised form 12 July 2023; Accepted 2 August 2023
Available online 5 August 2023

primary iron-bearing minerals into secondary iron-bearing minerals, which contributed to Cd redistribution. This study shows that SRB could exploit the composition and structure of minerals to induce mineral recrystallization, thereby aggravating Cd redistribution and immobilization in clay-size fractions from stratigraphic successions with high geochemical background.

1. Introduction

The mineral-microbial interface is a significant aspect of the Earth's critical zone, in which fundamental chemical transformations occur (Zhu et al., 2014). The amount of metallic elements (e.g. Cd) present in minerals is a regulating factor in the growth of microbes [29], and microbes, in turn, alter the cycle of metallic elements through their metabolic activities [10,46]. High geochemical background is a phenomenon in which the enrichment of heavy metals is attributed to the soil-forming parent rock and its weathering process, rather than anthropogenic factors [60]. Areas with high geochemical background can experience differential weathering, leading to an increase in the amount of heavy metals, especially Cd, in the soil. This is of great concern due to Cd's ecological toxicity. Moreover, elevated Cd in the soil can cause health issues, including renal failure and olfactory impairment, through biochemical cycles [14,16,48,60]. Biomineralization is an effective way to deactivate Cd in the soil and decrease the bioavailability of Cd [24]. It takes advantage of the complex interplay between minerals and microbes, representing an environmentally friendly approach [22].

In paddy field with high geochemical background, sulfate-reducing bacteria (SRB) are found in abundance in the reducing environment of rice rhizosphere. It exhibits strong interaction with minerals in soil, which enables them to immobilize cadmium (Cd) in the soil by reducing its bioavailability through biomineralization [28,38,40,62]. By utilizing organic matter as a carbon source and electron donor, SRB transform SO_4^{2-} as the terminal electron acceptor into various sulfide forms (H_2S, HS^-, S^{2-}) as their respiratory products [20,23]. To immobilize heavy metals in soil, SRB can utilize S^{2-} to precipitate metals and form metal sulfides with low solubility [1,12,63]. Therefore, by exploiting the physiological functioning of SRB and the distinctive nature of Cd in the soil, biomineralization through SRB can be a viable solution to address Cd contamination.

Clay-size fractions are highly absorbent, and thus they are most likely to contain Cd. Clay minerals and iron-bearing minerals are the two main elements responsible for this. Clay minerals in soil not only act as a sink for heavy metals but also render them inert [26,42]. The iron-bearing minerals in the clay-size fractions are able to reduce Cd's mobility with the assistance of microbes [34]. Take *Geobacter* as an example, during the continuous microbial reaction process, Fe(III) is reduced to Fe(II), resulting in either Fe(II) or a mixture of Fe(III) and Fe (II) secondary minerals [37], while Cd is captured in the secondary iron-bearing minerals [53]. When clay minerals interact with iron-bearing minerals, they form clay-size fractions that have a stable structure and a large specific surface area, which can adsorb a majority of the Cd in the soil. The varying weathering of parent rocks in strata results in disparity in physiochemical properties of developed soils, including the mineralogical composition and clay content [54]. Further the exact mechanism of how Cd in clay-size fractions is transformed by co-existing iron-bearing minerals and SRB has not been well illustrated. Therefore, it is necessary to explore the effectiveness of SRB in immobilizing Cd in clay-size fractions under various lithology backgrounds with high geochemical background of Cd.

In this study, we created a model system to explore the role of SRB in determining the fate of Cd in soils with high geochemical background from different stratigraphic successions. The soil samples were obtained from profiles of purple soils in the karst area of southwest China, and were rich in clay-size fractions and Cd. Clay-size fractions, and two iron oxide phases, i.e., amorphous iron oxides (Fe_{-OX}) and crystallized iron oxides (Fe_{-CBD}), were technically extracted from the soil samples and then subjected to reaction with SRB. To reveal the underlying mechanism, sequential extraction, X-ray diffraction (XRD) and X-ray photoelectron spectroscopy (XPS) were adopted to characterize Cd fractionation and primary/secondary minerals in the original samples and reaction products. This study provided a reference for better understanding the mobility and fate of heavy metals in soils with high geochemical background.

2. Materials and methods

2.1. Study area

The information of soil sampling sites is shown in Fig. 1. Soil samples with high geochemical background were collected from the northwest of Xiushan country, Chongqing (108°43′6″−109°18′58″E, 28°9′43″−28°53′5″N), southwestern China. A total of 20 soil samples were collected from 7 different surface layers of cultivated land, with strata being Nanhua (3 samples), Sinian (2 samples), Cambrian (3 samples), Ordovician (3 samples), Silurian (5 samples), Permian (2 samples), and Triassic (2 samples), respectively. The physical and chemical properties of soil samples are shown in Table 1.

The parent rocks of Nanhua, Silurian and Ordovician strata are silicate rocks, mainly including sandstone, shale and mudstone, whereas the carbonate rocks of Cambrian, Triassic and Sinian strata are mainly dolomite and limestone. Unlike other strata, the parent rocks of the Permian stratum contain a mixture of chert and limestone (Table 2). Soil Cd concentration in the region (Table 1) exceeded the Chinese Soil Environmental Quality Standard (GB15618–2018). It is a representative area of abnormal soil Cd enrichment from geogenic source, i.e., high geochemical background. After collection, the soil samples were air-dried and passed through a 10-mesh (2 mm diameter) sieve to remove debris and pebbles.

2.2. Extraction of clay-size fractions from soils

The clay-size fractions (particle size <2 μm) in the soil samples were extracted according to Ji et al. [15], and then 30% H_2O_2 was used to remove organic matter from the clay-size fractions.

2.3. Construction of the SRB-clay model system

The SRB-clay model system was constructed consisting of the SRB and the clay-sized fractions of soils to explore the redistribution and immobilization of Cd in soils. Firstly, SRB were isolated and purified from the bulk of purple paddy soil according to the method of Li et al. [25] and the DNA homology comparison was performed to verify the identity of the single strain. The SRB were then cultured in a modified Postgate liquid medium [41] until they reached the log phase, resulting in the SRB fluid. The Postgate liquid medium consists of NaCl 2.0 g/L, NH_4Cl 1.0 g/L, $MgSO_4{\cdot}7\ H_2O$ 2.0 g/L, Na_2SO_4 0.5 g/L, K_2HPO_4 0.5 g/L, 70% sodium lactate 5 mg/L, yeast extract 1.0 g/L, $FeSO_4$ 0.2 g/L, ascorbic acid 0.1 g/L, and L-cysteine 0.5 g/L, and the pH of the medium was adjusted to 7.0. To ensure sterility, ascorbic acid and L-cysteine were subjected to 30 min of UV light sterilization, followed by dissolution in sterile water via a 0.22-μm filter, and subsequent addition to the autoclaved medium. To initial the reaction of the SRB-clay model system, 150 mg of clay-size fractions were placed into a 25-mL culture medium and sterilized. Then the SRB fluid was introduced at a volume

ratio of 1:25, and the reaction system was placed in an anaerobic environment within an incubator at 35 °C for 10 days. Following this, the resulting pellets were centrifuged and dried in an oven at 45 °C. The Cd concentration in the supernatant suspension was determined by inductively coupled plasma mass spectrometry (ICP-MS).

2.4. Extraction of iron-bearing minerals phase

Taking the clay-size fraction weathered from the Triassic stratum and their products after adding SRB as an example, two types of iron minerals, i.e., amorphous iron oxide (Fe_{-OX}), crystallized iron oxide (Fe_{-CBD}) were extracted following an established procedure [25,30]. Initially, the extractant was prepared with 1 M hydroxylamine hydrochloride ($NH_2OH{\cdot}HCl$) and 25% (v/v) acetic acid, and the reaction was conducted with a ratio of 50 mL extractant per 100 mg clay-size fractions. The mixture was shaken 3 times at a 30-min interval for 10 min each, and kept in the dark for 24 h to yield amorphous iron oxides (Fe_{-OX}) [5]. To further obtain Fe_{-CBD} (citrate-bicarbonate-dithionite), Fe_{-OX} was placed in a water bath at 80 °C and mixed with 45 mL sodium citrate (0.3 M), 5 mL sodium bicarbonate (1 M) and a surplus of sodium bisulfite powder for 30 min [33].

2.5. Characterization of Cd fractions and mineral phases in the SRB-clay system

Fractions of Cd in the original clay-size fractions, Fe_{-OX}, and Fe_{-CBD}, and their reaction products with SRB were extracted by the Tessier method [49]. The method defines 5 fractions of Cd, i.e., exchangeable fraction (F1), carbonate binding fraction (F2), iron/manganese oxide binding fraction (F3), organic binding fraction (F4), and residual fraction (F5). To keep the error range within similar limits, equal amounts of chemical extractants were used for both the pre-reaction clay-size fraction and post-reaction products. Analytical duplicates and blanks were included to ensure the precision and accuracy of the results. XRD analysis (Bruker D8 Advance, German) was performed on original clay-size fractions, and their reaction products with SRB to analyze the changes in clay mineral phase. FTIR spectra of functional group changes in clay-size fractions, Fe_{-OX}, $F_{e\text{-}CBD}$ and their products after adding SRB were recorded using an FTIR spectrometer (Nicolet 6700, Thermo Fisher Scientific, USA) equipped with a KBr beam splitter and a DTGS detector. XPS is a reliable technique for comprehending the alterations in minerals upon SRB addition. Hence, the Fe_{-OX}, Fe_{-CBD}, and their resultant products were subjected to XPS scanning (Shimazu-Kratos Analytical, UK), and the impact of iron-bearing minerals on the redistribution of Cd by SRB was evaluated by monitoring the changes in Fe functional groups.

2.6. Statistical analysis

Statistical analysis was carried out using SPSS 26.0 software. Pearson correlation analysis was performed to study the varying trend of Cd fractions. Significant difference in Pearson correlation coefficient were determined by Duncan's multiple range test at $p < 0.05$. The XRD patterns were analyzed using JADE 6.5 software package (MDI, USA), FTIR patterns were analyzed by Omnic 8.2, and XPS patterns were analyzed by combining Avantage and XPSspeak software. The spatial pattern in the information of sample site was visualized using ArcGIS 10.2 version software. In addition, data plotting and linear correlations were performed by using Origin 2021 software.

3. Results and discussion

3.1. Clay-size fractions were the primary reservoir for Cd

The Cd concentrations in soils and their clay-size fractions exhibited a marked variation (Fig. 2). The Cd concentration in soil was 0.24–2.84 mg/kg (avg = 0.81 mg/kg), which was much higher than the regional soil risk screening value (0.30 mg/kg). The clay-size fractions in the soil accounted for 6–13%, and the Cd content in these fractions was 4.08–6.77 mg/kg (avg = 5.12 mg/kg), which was 2–14 times higher than that in soils [31]. By analyzing the Cd concentration in the clay-size fractions and the proportion of clay-size fractions in the soil, we can know that clay-size fractions accumulated 23–65% of the Cd in the soil. These suggesting that clay-size fractions are the primary reservoir for Cd in soils [11,52].

The accumulation of Cd in soil was attributed to the different weathering of parent rocks, including carbonate and silicate parent rocks, causing the enrichment of Cd with high geochemical background [55,56]. Soils originating from carbonate parent rocks (Cambrian, Permian, Triassic, and Sinian) exhibited a considerably lower concentration of Cd ($T_{Cd\text{-}soil}$) in comparison to those originating from silicate parent rocks (Silurian, Ordovician, and Nanhua) (Fig. 2; Table 2). However, the concentration of Cd in clay-size fractions ($T_{Cd\text{-}clay}$) presented a contrasting pattern. The binding capacity of Cd in clay-size fractions of soils was dominated by properties of parent rock. Typically, trace metal (including Cd) concentration in carbonate rocks is lower than that in silicate rocks [44]. However, during the weathering of carbonate rocks, many highly soluble elements such as Ca and Mg are

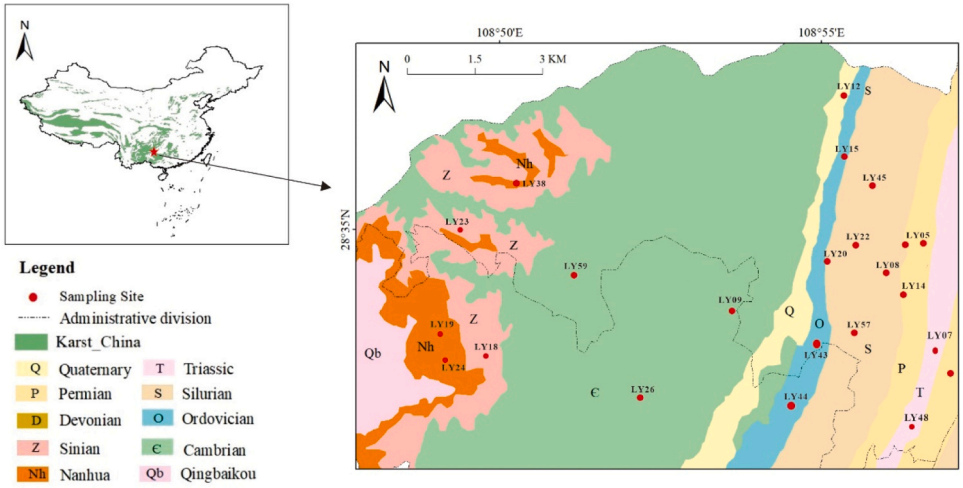

Fig. 1. Distribution map of weathered soil sampling sites in the northwest of Xiushan Country. Information regarding karst was sourced from the Karst Scientific Data Center (https:// www. karst data. cn/).

leached out, while low solubility elements like Cd are absorbed by clay minerals [51] and Fe-Mn oxides [64] in the clay size fractions. Consequently, the concentration of Cd in clay-size fractions in carbonate rocks is generally higher than in silicate rocks [55,56,58,57].

3.2. Redistribution of Cd in the SRB-clay system

Fig. 2 illustrates the changes in Cd concentration in soils and clay-size fractions following the introduction of SRB. The SRB-clay system experienced a decrease in Cd concentration from 4.08–6.77 mg/kg to 2.93–4.11 mg/kg . As indicated in Table 2, the highest reduction was observed in Cambrian (43.53%), while the lowest was in Permian (9.77%), followed by Silurian (21.61%). When further considering the properties of the parent rock (Table 2), it appears that SRB can more easily utilize clay-size fractions from carbonate rock than those from silicate mineral with compact structure [17,2].

Fig. 3 indicates that the fractions of Cd remained consistent across all parent materials, irrespective of the presence or absence of SRB. The implementation of SRB yielded changes in the Cd fractions, which were evident through a reduction in the levels of F1 and F2 fractions, and a considerable increase in the levels of F3 and F5 fractions (Fig. 3**(a)(b)**). Specifically, the level of F1 decreased from 1.56–3.63 mg/kg to 0.42–1.25 mg/kg, and F2 decreased from 0.85–1.56 mg/kg to 0.15–0.55 mg/kg to 0.15–0.55 mg/kg. Conversely, the level of F3 increased from 0.13-0.27 mg/kg to 1.40-3.21 mg/kg, and F5 increased from 0.31-1.04 mg/kg to 0.68-1.05 mg/kg. Moreover, the addition of SRB resulted in a negative correlation between F3 and F1 ($r = -0.650$, $p < 0.01$) and F2 ($r = -0.533$, $p < 0.05$) (Table S1). The bioavailability of Cd typically decreases as the sequential extraction progresses [7]. SRB may facilitate the release of Cd that was physically adsorbed on the surface of minerals (F1) or in carbonate minerals (F2), and further be immobilized by iron/manganese oxides (F3) or clay minerals (F5). This finding demonstrated that SRB were capable of effectively promoting the redistribution of Cd and reducing its bioavailability.

The occurrence of Cd in iron-bearing minerals is stabilized by the presence of iron-bearing phases, which have a significant effect on the immobilization of Cd and the catalytic production of crystalline iron minerals by SRB. The level of Cd in Fe_{-OX} was much higher than that in Fe_{-CBD} (0.25 vs 0.11 mg/kg). In Fe_{-OX}, Cd was predominantly occurred in the F1 and F2 fractions (79.67%), whereas in Fe_{-CBD}, it was also mainly present in the F1 and F3 fractions (50.88%) (Fig. 3(c)). Overall, the bioavailability of Cd in Fe_{-OX} was much higher than that in Fe_{-CBD}. When subjected to SRB, the concentration of Cd in Fe_{-OX} decreased sharply. Correspondingly, the concentration of Cd in Fe_{-CBD} displayed a substantial increase (Fig. 3(d)), indicating that SRB promoted the conversion of Cd from Fe_{-OX} to Fe_{-CBD}. Fe_{-OX} was primarily composed of easily reducible primary iron oxides, while Fe_{-CBD} was made up of crystalline primary iron oxides [30]. Fe_{-OX} is a potentially highly bioavailable nanocrystalline mineral with higher specific surface area and growth activity [36,43]. Due to its greater reducibility and bioavailability, SRB tends to utilize the Cd attributed to Fe_{-OX} and further recrystallize to generate secondary iron oxides, which are occurred mainly in Fe_{-CBD}. As a result, the level of Cd in Fe_{-CBD} was increased.

Within a span of 10 days of the model system's culture, a discernible alteration in the concentration and fractions of Cd within the clay-size fractions was observed. This phenomenon could be attributed to the utilization of minerals in the clay-size fractions as an energy source by SRB, thereby facilitating the transformation of the existing form of Cd in said minerals [45], leading to the redistribution of Cd in the soil [27]. Microbes (including SRB) can facilitate soil weathering through biomineralization [32], resulting in inevitably a certain amount of Cd release from solid phases [21]. Although SRB exhibit impressive resistance to Cd [39], this characteristic may exacerbate the sequestration of Cd in minerals, resulting in a further reduction in Cd solubility due to the formation of secondary minerals that are not easily accessible through physiological means [18]. In contrast to dense silicate rocks, carbonate rocks with high solubility were more attractive to SRB. As a result, the significant decrease in Cd concentration in the clay-size fractions of carbonate rocks after reaction with SRB was more pronounced than that of silicate rocks. The concentration of Cd in the clay-size fractions of both carbonate rocks and silicate rocks tends to be uniform following reaction with SRB, as SRB had effectively retained most Cd in the

Table 2
Lithology in the study area, and Cd concentration in soils and clay-size fractions.

System	Lithology in study area	Cd concentration in soils (mg/kg)	Cd concentration in clay-size fractions (mg/kg)	Cd decrease rate (wt%)
Cambrian	Dolomite	0.86 (± 0.23)	5.61 (± 0.82)	37.21
Triassic	Dolomite	0.41 (± 0.06)	5.57 (± 0.32)	30.36
Permian	Flint, Limestone	0.65 (± 0.08)	4.86 (± 0.26)	9.77
Ordovician	Shale	0.98 (± 0.64)	5.15 (± 0.28)	26.03
Silurian	Mudstone Shale	1.06 (± 0.90)	4.78 (± 0.44)	21.61
Sinian	Dolomite	0.32 (± 0.08)	5.56 (± 0.09)	34.57
Nanhua	Sandstone Shale	0.91(± 0.13)	5.37 (± 0.41)	26.12

Table 1
Physical and chemical properties of soils in different strata of Xiushan.

Name	stratum	Code name	Cd (mg/kg)	Mn (mg/kg)	pH	Fe_2O_3 (wt%)	CaO (wt%)	OC (wt%)
LY05	Permian	P_2m	0.57	1196.50	6.66	4.91	0.61	1.35
LY14	Permian	P_3w	0.73	2510.20	6.00	5.55	0.36	1.28
LY08	Silurian	$S_1hx^{,1}$	0.37	1236.90	6.91	8.03	0.56	1.34
LY20	Silurian	$S_1hx^{,2}$	0.94	1141.50	6.78	5.63	2.13	1.20
LY22	Silurian	S_1x	0.56	1293.80	6.73	5.36	1.07	1.69
LY45	Silurian	$S_1xs^{,1}$	2.84	1037.00	6.43	4.57	0.32	1.01
LY57	Silurian	$S_1xs^{,2}$	0.60	399.70	6.66	4.43	0.41	1.10
LY07	Triassic	$T_1d^{,1}$	0.35	263.50	6.81	3.98	0.52	1.94
LY48	Triassic	$T_1d^{,2}$	0.47	1401.10	6.28	4.43	0.30	1.40
LY18	Sinian	$Z_1d+Z_2ds^{,1}$	0.41	319.20	4.94	5.42	0.16	0.79
LY23	Sinian	$Z_1d+Z_2ds^{,2}$	0.24	390.90	5.25	5.53	0.18	0.97
LY15	Ordovician	O_1d	1.83	177.90	5.83	5.70	0.21	1.04
LY43	Ordovician	O_1n	0.27	415.00	4.79	4.73	0.16	1.19
LY44	Ordovician	O_2	0.84	1016.30	4.99	4.11	0.18	1.19
LY19	Nanhua	$Nh_2n^{,1}$	0.72	195.60	5.25	3.98	0.20	1.44
LY24	Nanhua	$Nh_2n^{,2}$	0.97	982.00	5.83	6.22	0.25	1.11
LY38	Nanhua	Nh_2d	1.04	1031.00	6.48	6.31	0.50	1.44
LY09	Cambrian	ϵ_2s	0.75	942.30	6.15	6.41	0.32	0.95
LY26	Cambrian	ϵ_3g	1.19	354.40	5.66	5.95	0.19	0.96
LY59	Cambrian	ϵ_3m	0.66	864.30	6.50	5.38	3.09	3.20

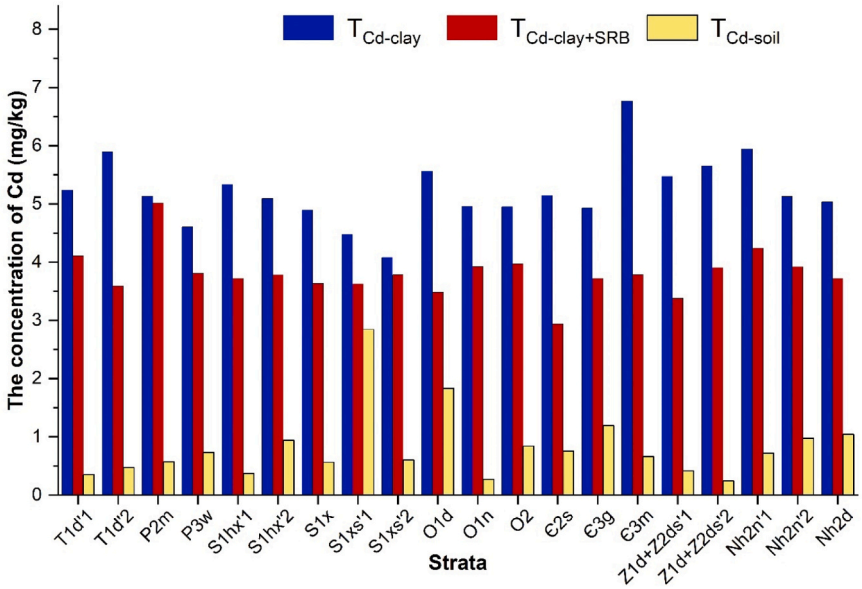

Fig. 2. The Cd contents in the native soils ($T_{Cd\text{-}soil}$), the extracted clay-size fractions for SRB reaction ($T_{Cd\text{-}clay}$) and the resulting clay-size fractions after SRB reaction ($T_{Cd\text{-}clay+SRB}$).

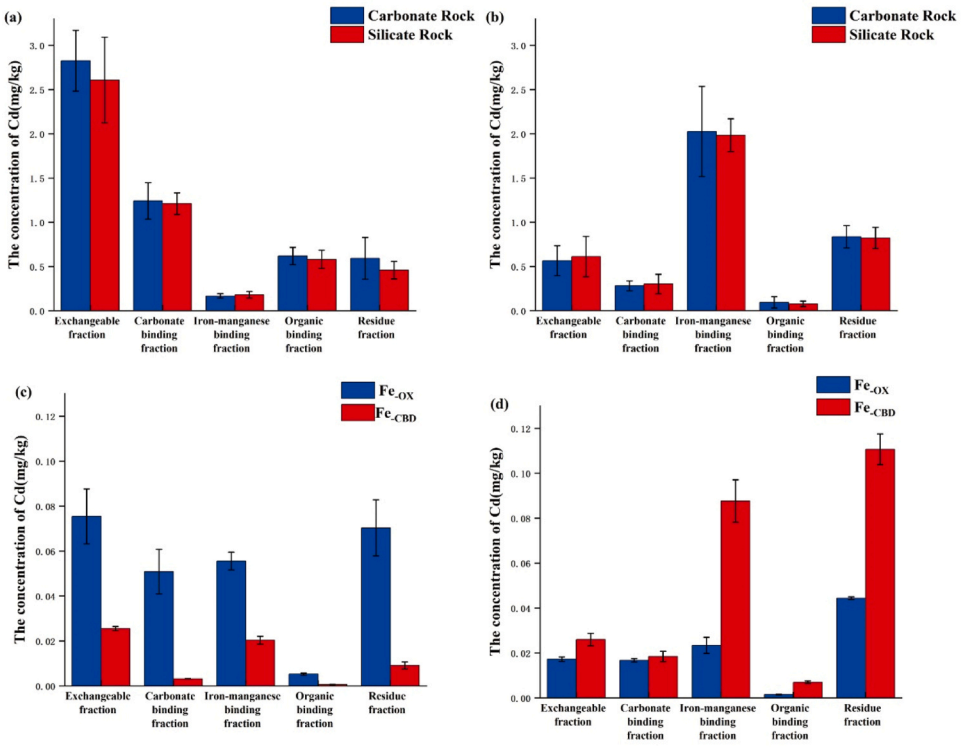

Fig. 3. Changes in Cd fractions in clay-size fractions before and after SRB reaction. (a) the level of five Cd fractions in the original soil clay-size fractions, (b) the level of five Cd fractions in the products after the introduction of SRB, (c) the level of five Cd fractions in $Fe_{\text{-}OX}$ and $Fe_{\text{-}CBD}$ in the original soil clay-size fractions, and (d) the level of five Cd fractions in $Fe_{\text{-}OX}$ and $Fe_{\text{-}CBD}$ after the introduction of SRB. F1, F2, F3, F4 and F5 denote the exchangeable fraction, carbonate bound, Fe-Mn bound, organic bound, and residue fractions, respectively.

clay-size fractions.

3.3. Mineral transformation in the SRB-clay system

To understand the change of mineral phases during biomineralization process induced by SRB, the clay-size fractions and products in SRB-clay system by XRD were carried out (Fig. 4 (a)). Illite, kaolinite, and chlorite were primarily present in the clay-size fractions of weathering soil samples from stratigraphic successions, and their production was leached by SRB (Fig. 4 (a); Fig. S1). XRD patterns of the samples in the SRB-clay system revealed that the peak height and half-peak width of different phases decreased after SRB reaction ($\Delta H > 0$, $\Delta FWHM > 0$) (Table S2). This indicated a reduction in the content of illite, kaolinite, chlorite and other clay minerals, and a decrease in the degree of crystallization [9]. The vanishing peak at $2\theta = 37.8°$ can be ascribed to the dissolution of the characteristic iron-bearing minerals in the clay-size fractions, which is a result of the active involvement of SRB in its transformation process.

FTIR was used to analyze the changes of functional groups in clay-size fractions, $Fe_{\text{-}OX}$ and $Fe_{\text{-}CBD}$ during chemical extraction and SRB culturing (Fig. 4(b)). The absorption peak shapes of the FTIR spectra for clay-size fractions, $Fe_{\text{-}OX}$ and $Fe_{\text{-}CBD}$ were similar. The peak lines for $Fe_{\text{-}}$

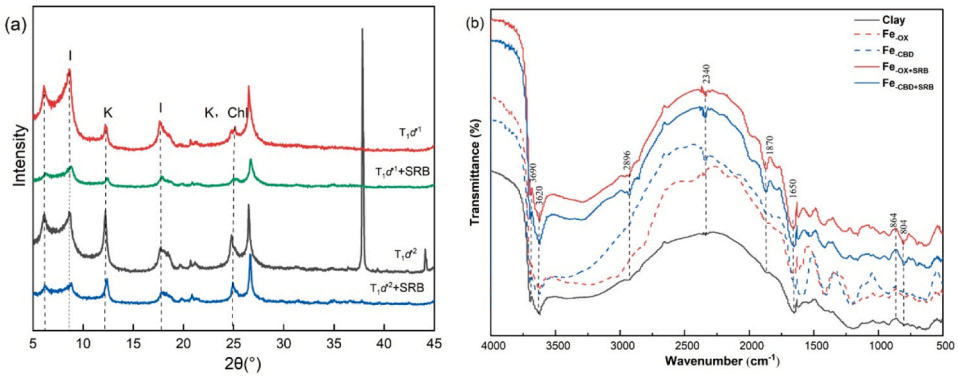

Fig. 4. XRD patterns (a) and FTIR spectra (b) for clay-size fractions or iron minerals before and after reaction with SRB. I, illite; K, kaolinite; Ch, chlorite. Fe_{-OX}, amorphous iron oxide; Fe_{-CBD}, crystallized iron oxide; $Fe_{-OX+SRB}$, Fe_{-OX} after reaction with SRB; $Fe_{-CBD+SRB}$, Fe_{-CBD} after reaction with SRB.

$_{OX}$ and Fe_{-CBD} had close transmittance and even overlap at 1650–864 cm^{-1}, indicating that the chemical extraction process has litter effect on functional groups. In the wavenumber of 3690–3620 cm^{-1}, deep and narrow absorption peaks were observed, which were due to the vibration of Al-O bonds in the clay minerals. Strong and broad peaks at 2900–3500 cm^{-1} were attributed to the O-H stretching vibration. After SRB was added, several new peaks appeared, such as at 2896, 1870, and 804 cm^{-1}, suggesting that the bacterial culture had a major impact on the functional groups during the immobilization of Cd. According to Soriano-Disla et al. [47], the peak at 2896 cm^{-1} is a C-H bond stretching vibration in organic matter, and the peak at 804 cm^{-1} is associated with secondary iron-bearing minerals, whereas, the peak at 1870 may be related to secondary Cd-bearing minerals, i.e., CdS or Cd-Fe coprecipitation [63].

Fig. 5 illustrates the changes in the Fe(III)/Fe(II) mineral components of Fe_{-OX} and Fe_{-CBD} as determined by XPS analysis before and after the inclusion of SRB. The full spectrum showed the manifestation of Cd3d and S2p orbitals, which may indicate the formation of the secondary mineral of greenockite (CdS) [63,65]. The fine spectrum of Fe displayed two spectral peaks of Fe 1/2p and Fe 3/2p, which were situated at binding energies of 726.08–726.98 eV and 711.38–712.08 eV, respectively. The peak area of Fe^{3+} in Fe_{-OX} was much higher than that of Fe_{-CBD}, indicating that the concentration of Fe^{3+} in Fe_{-OX} was higher than that of Fe_{-CBD}. Comparison of the peak area of Fe^{3+} and Fe^{2+} at Fe 3/2p showed that the ratio (the area value of Fe^{3+}/ the area value of Fe^{2+}) in Fe_{-OX} decreased (from 1.52 to 1.31) after SRB addition, confirming that some Fe^{3+} was reduced to Fe^{2+}. In Fe_{-CBD}, the peak area of Fe^{3+} and Fe^{2+} showed an opposite trend, and the ratio of peak area increased (from 1.06 to 1.53), but the peak area value was much smaller than when SRB was added (Table S3). These results verified that SRB favored Fe_{-OX} over Fe_{-CBD}, leading to the reduction of Fe^{3+} to Fe^{2+} and subsequent formation of secondary iron oxides [59]. The secondary iron oxides may be present mainly in the form of Fe-CBD, thereby increasing the concentration of Cd in Fe_{-CBD} (Fig. 3(c)(d)).

3.4. Mechanism of Cd immobilization in the SRB-clay system

According to the level of Cd fraction and XRD, FTIR and XPS analyses, it can be inferred that under anaerobic conditions, the immobilization of Cd on mineral surfaces occurred through the activity of SRB. This process was accompanied by the release of extracellular enzymes and other substances that facilitated the desorption of Cd^{2+} from unstable carbonate minerals. A significant amount of Cd^{2+} was initially released from unstable primary minerals (including F1 and F2 fractions) by SRB, and subsequently adsorbed in the interlayer of clay minerals. Over time, clay minerals became the primary site for SRB to immobilize Cd, leading to further structural degradation of the clay minerals. The surface of the destroyed clay minerals contains hydroxyl groups [35], which may provide surface adsorption sites for Cd^{2+} and promote the immobilization of Cd^{2+} in F5 fraction, resulting in an increased proportion of this fraction (Fig. 3(a)(b)).

When Cd in unstable primary minerals reach the dissolution limit, the initial co-precipitation of Cd and Fe (design as F3) dissolves and releases Cd^{2+} and Fe^{3+}. SRB utilize Fe^{3+} as the electron acceptor, converting it to Fe^{2+} [20]. Subsequently, the reduced Fe^{2+} forms secondary Fe(II) minerals with S^{2-} and CO_3^{2-}, i.e., FeS and $FeCO_3$ respectively [6,8,25]. Some Fe^{2+} interacted with Fe^{3+} forms Fe(III)/FeII) mixed iron minerals phase, such as magnetite (Fe_3O_4) [4]. The above minerals further stimulated the activity of SRB (Bratcova, S et al., 2002), leading to an acceleration in the rate of destroying of the structure of primary crystalline iron oxides. Additionally, electron transfer or atomic replacement [42,50] causes the transformation of the co-precipitation

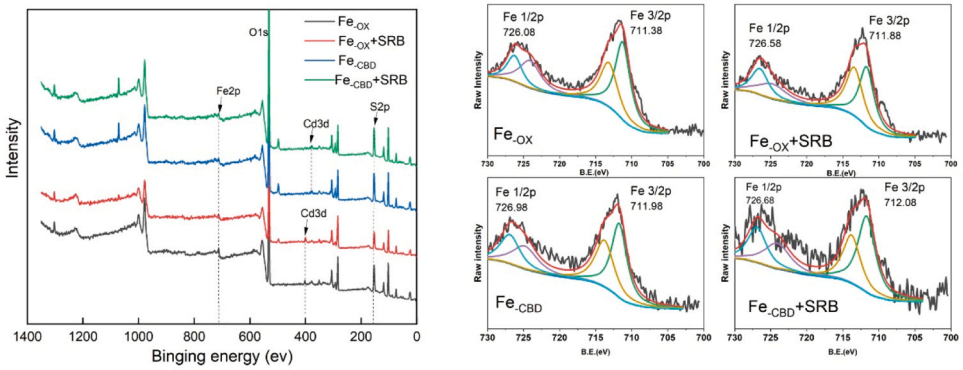

Fig. 5. XPS spectra before and after the reaction of different iron-bearing minerals with SRB. Left is full spectrum, right is Fe fine spectrum, green and purple peak lines are Fe^{3+}, blue and yellow peak lines are Fe^{2+}.

into iron-bearing crystalline minerals, which in turn leads to the formation of secondary iron-bearing minerals [25]. In the SRB-clay system, these secondary minerals provided abundant binding sites for Cd^{2+} with a high affinity [19,3], ultimately promoting the immobilization of Cd^{2+} by secondary iron-bearing minerals. During the formation of secondary iron oxide minerals, uncoordinated Cd^{2+} may be attracted to form secondary Cd-Fe co-precipitation, immobilizing Cd^{2+} in iron-bearing compounds [53]. Since the Cd-Fe co-precipitates had a large specific surface area [61], they can absorb a high amount of Cd by recrystallization and increase the proportion of Cd in iron-containing minerals (Fig. 3).

This study's results were mainly based on controlled experiments with specially designed reaction systems. To further understand the role of SRB in aiding the mineral conversion of iron oxides and the immobilization of Cd in soils in natural settings, more efforts are necessary. This necessitates the implementation of in-situ characterization methods for elements [13], minerals and microbes, and/or novel strategies such as synthetic biology.

4. Conclusions

The constructed SRB-clay system can be used as a model system for exploring the redistribution and immobilization of Cd in soils with high geochemical background. The structure and weathering susceptibility of the parent rock had a major influence on Cd levels in soils and their clay components from stratigraphic successions, as well as the effectiveness of SRB in immobilizing Cd in the clay-size fractions. Nevertheless, it is noteworthy that these properties did not affect the fractionation of Cd. SRB caused the redistribution of Cd in the clay-size fractions, which exhibited a high adsorption capacity for Cd^{2+} and were the primary site of Cd activation by SRB. Moreover, the process of Cd immobilization by SRB disrupted the stable structure of clay minerals. SRB tended to utilize clay-size fractions from carbonate rock derived soils, not silicate rock derived soils. Iron-bearing minerals stimulated SRB to accelerate Cd immobilization. Furthermore, the efficiency of SRB in immobilizing Cd was affected by the type of iron mineral phase present, with $Fe_{\cdot OX}$ being more favorable due to its stronger reducing properties compared to $Fe_{\cdot CBD}$.

CRediT authorship contribution statement

Xing Yan: Visualization, Investigation, Formal analysis, Writing – original draft. **Dong-Xing Guan**: Conceptualization, Methodology, Supervision, Writing – review& editing. **Jie Li:** Investigation, Methodology. **Yinxian Song:** Supervision; Validation. **Hua Tao** : Resources, Investigation. **Xianming Zhang:** Conceptualization. **Ming Ma:** Resources. **Junfeng Ji:** Supervision, Resources, **Wancang Zhao**: Conceptualization, Data curation, Writing – review & editing, Funding acquisition, Supervision.

Declaration of Competing Interest

The authors declare that they have no known competing financial interests or personal relationships that could have appeared to influence the work reported in this paper.

Data availability

Data will be made available on request.

Acknowledgements

This work was funded by the National Natural Science Foundation of China (42177194 and 41673095), and the Fundamental Research Funds for the Central Universities (2021QNA6004).

Appendix A. Supporting information

Supplementary data associated with this article can be found in the online version at doi:10.1016/j.jhazmat.2023.132213.

References

[1] Ayala-Parra, P., Sierra-Alvarez, R., Field, J.A., 2016. Treatment of acid rock drainage using a sulfate-reducing bioreactor with zero-valent iron. J Hazard Mater 308, 97–105.
[2] Barker, J.S., Tagu, D., Delp, G., 1998. Regulation of root and fungal morphogenesis in mycorrhizal symbioses1. Plant Physiol 116 (4), 1201–1207.
[3] Bolton, K.A., Evans, L.J., 1996. Cadmium adsorption capacity of selected Ontario soils. Can J Soil Sci 76 (2), 183–189.
[4] Borch, T., Kretzschmar, R., Kappler, A., Cappellen, P.V., Ginder-Vogel, M., Voegelin, A., et al., 2010. Biogeochemical redox processes and their impact on contaminant dynamics. Environ Sci Technol 44 (1), 15–23.
[5] Chen, Y., Siefert, R.L., 2003. Determination of various types of labile atmospheric iron over remote oceans. J Geophys Res: Atmospheres 108 (D24), 4774.
[6] Cohen, R.R.H., 2006. Use of microbes for cost reduction of metal removal from metals and mining industry waste streams. J Clean Prod 14 (12–13), 1146–1157.
[7] Ding, S., Guan, D., Dai, Z., Su, J., Teng, H.H., Ji, J., et al., 2022. Nickel bioaccessibility in soils with high geochemical background and anthropogenic contamination. Environ Pollut 310, 119914.
[8] Enning, D., Garrelfs, J., 2014. Corrosion of iron by sulfate-reducing bacteria: new views of an old problem. Appl Environ Microbiol 80 (4), 1226–1236.
[9] Esnault, L., Libert, M., Bildstein, O., Mustin, C., Marsal, F., Jullien, M., 2013. Impact of iron-reducing bacteria on the properties of argillites in the context of radioactive waste geological disposal. Appl Clay Sci 83–84, 42–49.
[10] Fredrickson, J.K., Zachara, J.M., 2008. Electron transfer at the microbe–mineral interface: a grand challenge in biogeochemistry. Geobiology 6 (3), 245–253.
[11] Gankhurel, B., Fukushi, K., Akehi, A., Takahashi, Y., Zhao, X., Kawasaki, K., 2020. Comparison of chemical speciation of lead, arsenic, and cadmium in contaminated soils from a historical mining site: implications for different mobilities of heavy metals. ACS Earth Space Chem 4 (7), 1064–1077.
[12] Geets, J., Vanbroekhoven, K., Borremans, B., Vangronsveld, J., Diels, L., van der Lelie, D., 2006. Column experiments to assess the effects of electron donors on the efficiency of in situ precipitation of Zn, Cd, Co and Ni in contaminated groundwater applying the biological sulfate removal technology. Environ Sci Pollut Res Int 13 (6), 362–378.
[13] Guan, D.X., He, S.X., Li, G., Teng, H.H., Ma, L.Q., 2022. Application of diffusive gradients in thin-films technique for speciation, bioavailability, modeling and mapping of nutrients and contaminants in soils. Crit Rev Environ Sci Technol 52 (17), 3035–3079.
[14] Guo, C., Wen, Y., Yang, Z., Li, W., Guan, D., Ji, J., 2019. Factors controlling the bioavailability of soil cadmium in typical karst areas with high geogenic background. J Nanjing Univ Nat Sci 55 (4), 678–687.
[15] Ji, J., Chen, J., Lu, H., 1999. Origin of illite in the loess from the Luochuan area, Loess Plateau, central China. Clay Miner 34 (4), 525–532.
[16] Jia, Z., Wang, J., Zhou, X., Zhou, Y., Li, Y., Li, B., et al., 2020. Identification of the sources and influencing factors of potentially toxic elements accumulation in the soil from a typical karst region in Guangxi, Southwest China. Environ Pollut 256, 113505.
[17] Jones, A.A., Bennett, P.C., 2017. Mineral ecology: surface specific colonization and geochemical drivers of biofilm accumulation, composition, and phylogeny. Front Microbiol 8.
[18] Karna, R., Hettiarachchi, G., Van Nostrand, J., Yuan, T., Rice, C., Assefa, Y., et al., 2018. Microbial Population Dynamics and the Role of Sulfate Reducing Bacteria Genes in Stabilizing Pb, Zn, and Cd in the Terrestrial Subsurface. Soil Systems 2 (4), 60.
[19] Ke, C., Guo, C., Zhang, S., Deng, Y., Li, X., Li, Y., et al., 2023. Microbial reduction of schwertmannite by co-cultured iron- and sulfate-reducing bacteria. Sci Total Environ 861, 160551.
[20] Ko, M., Park, H., Lee, J., 2017. Influence of indigenous bacteria stimulation on arsenic immobilization in field study. Catena 148, 46–51.
[21] Kolowith, L.C., Berner, R.A., 2002. Weathering of phosphorus in black shales. Glob Biogeochem Cycles 16 (4), 81–87.
[22] Kratochvil, D., Volesky, B., 1998. Advances in the biosorption of heavy metals. Trends Biotechnol 16 (7), 291–300.
[23] Kumar, M., Nandi, M., Pakshirajan, K., 2021. Recent advances in heavy metal recovery from wastewater by biogenic sulfide precipitation. J Environ Manag 278, 111555.
[24] Li, F., Wang, W., Li, C., Zhu, R., Ge, F., Zheng, Y., et al., 2018. Self-mediated pH changes in culture medium affecting biosorption and biomineralization of Cd2+ by Bacillus cereus Cd01. J Hazard Mater 358, 178–186.
[25] Li, J., Zhao, W., Du, H., Guan, Y., Ma, M., Rennenberg, H., 2022. The symbiotic system of sulfate-reducing bacteria and clay-sized fraction of purplish soil strengthens cadmium fixation through iron-bearing minerals. Sci Total Environ 820, 153253.
[26] Li, Y., Dong, S., Qiao, J., Liang, S., Wu, X., Wang, M., et al., 2020. Impact of nanominerals on the migration and distribution of cadmium on soil aggregates. J Clean Prod 262, 121355.

[27] Liu, Y., Xiao, T., Zhu, J., Gao, T., Xiong, Y., Zhu, Z., et al., 2022. Redistribution and isotope fractionation of endogenous Cd in soil profiles with geogenic Cd enrichment. Sci Total Environ 852, 158447.
[28] Liu, Z., Yang, S., Bai, Y., Xiu, J., Yan, H., Huang, J., et al., 2011. The alteration of cell membrane of sulfate reducing bacteria in the presence of Mn(II) and Cd(II). Miner Eng 24 (8), 839–844.
[29] Lower, S.K., Tad, C.J., 2001. Dynamics of the mineral-microbe interface: use of biological force microscopy in biogeochemistry and geomicrobiology. Geomicrobiol J 18 (1), 63–76.
[30] Lu, W., Zhao, W., Balsam, W., Lu, H., Liu, P., Lu, Z., et al., 2017. Iron mineralogy and speciation in clay-sized fractions of chinese desert sediments. J Geophys Res Atmos 122 (24), 413–458, 13.
[31] Luo, X., Wang, Z., Lu, C., Huang, R., Wang, F., Gao, M., 2019. Effects of land use type on the content and stability of organic carbon in soil aggregates. Environ Sci 40 (8), 3816–3824.
[32] Mahaney, W.C., Krinsley, D.H., Allen, C.C.R., 2013. Biomineralization of weathered rock rinds; examples from the lower Afroalpine Zone on Mount Kenya. Geomicrobiol J 30 (5), 411–421.
[33] Mehra, O.P., Jackson, M.L., 1958. Iron oxide removal from soils and clays by a dithionite citrate system buffered with sodium bicarbonate. Clay Clay Miner 7 (1), 317–327.
[34] Mello Gabriel, G.V., Pitombo, L.M., Rosa, L.M.T., Navarrete, A.A., Botero, W.G., Do Carmo, J.B., et al., 2021. The environmental importance of iron speciation in soils: evaluation of classic methodologies. Environ Monit Assess 193 (2).
[35] Michalkova, A., Johnson, L.D., Gorb, L., Zhikol, O.A., Shishkin, O.V., Leszczynski, J., 2005. Theoretical study of adsorption of methyltert-butyl ether on broken clay minerals surfaces. Int J Quantum Chem 105 (4), 325–340.
[36] Michel, F.M., Ehm, L., Antao, S.M., Lee, P.L., Chupas, P.J., Liu, G., et al., 2007. The structure of ferrihydrite, a nanocrystalline material. Science 316 (5832), 1726–1729.
[37] Muehe, E.M., Obst, M., Hitchcock, A., Tyliszczak, T., Behrens, S., Schroder, C., et al., 2013. Fate of Cd during microbial Fe(III) mineral reduction by a novel and Cd-Tolerant Geobacter species. Environ Sci Technol 47 (24), 14099–14109.
[38] Muyzer, G., Stams, A.J.M., 2008. The ecology and biotechnology of sulphate-reducing bacteria. Nat Rev Microbiol 6 (6), 441–454.
[39] Naz, N., Young, H.K., Ahmed, N., Gadd, G.M., 2005. Cadmium accumulation and DNA homology with metal resistance genes in sulfate-reducing bacteria. Appl Environ Microbiol 71 (8), 4610–4618.
[40] Peng, W., Li, X., Liu, T., Liu, Y., Ren, J., Liang, D., et al., 2018. Biostabilization of cadmium contaminated sediments using indigenous sulfate reducing bacteria: Efficiency and process. Chemosphere 201, 697–707.
[41] Postgate, J.R., Campbell, L.L., 1966. Classification ofdesulfovibrio species, the nonsporulating sulfate-reducing bacteria. Bacteriol Rev 30 (4), 732–738.
[42] Qian, J., Shan, X., Wang, Z., Tu, Q., 1996. Distribution and plant availability of heavy metals in different particle-size fractions of soil. Sci Total Environ 187 (2), 131–141.
[43] Raiswell, R., Vu, H.P., Brinza, L., Benning, L.G., 2010. The determination of labile Fe in ferrihydrite by ascorbic acid extraction: Methodology, dissolution kinetics and loss of solubility with age and de-watering. Chem Geol 278 (1), 70–79.
[44] Salomons, W., Förstner, U., 2012. Metals in the Hydrocycle. Springer Science &Business Media,.
[45] Shan, S., Guo, Z., Lei, P., Wang, Y., Li, Y., Cheng, W., et al., 2019. Simultaneous mitigation of tissue cadmium and lead accumulation in rice via sulfate-reducing bacterium. Ecotoxicol Environ Saf 169, 292–300.
[46] Sokol, N.W., Slessarev, E., Marschmann, G.L., Nicolas, A., Blazewicz, S.J., Brodie, E.L., Firestone, M.K., Foley, M.M., Hestrin, R., Hungate, B.A., Koch, B.J., Stone, B. W., Sullivan, M.B., Zablocki, O., & Pett-Ridge, J. (2022). Life and death in the soil microbiome: how ecological processes influence biogeochemistry [Journal Article; Research Support, U.S. Gov't, Non-P.H.S.; Review]. Nature Reviews Microbiology, 20(7), 415–430.
[47] Soriano-Disla, J.M., Janik, L.J., Viscarra rossel, R.A., Macdonald, L.M., Mclaughlin, M.J., 2014. The performance of visible, near-, and mid-infrared reflectance spectroscopy for prediction of soil physical, chemical, and biological properties. Appl. Spectrosc. Rev. 49 (2), 139–186.
[48] Tabelin, C.B., Igarashi, T., Villacorte-Tabelin, M., Park, I., Opiso, E.M., Ito, M., et al., 2018. Arsenic, selenium, boron, lead, cadmium, copper, and zinc in naturally contaminated rocks: A review of their sources, modes of enrichment, mechanisms of release, and mitigation strategies. Sci Total Environ 645, 1522–1553.
[49] Tessier, A., Campbell, P.G.C., Bisson, M., 1979. Sequential extraction procedure for the speciation of particulate trace metals. Anal Chem (Wash) 51 (7), 844–851.
[50] Tomaszewski, E.J., Olson, L., Obst, M., Byrne, J.M., Kappler, A., Muehe, E.M., 2020. Complexation by cysteine and iron mineral adsorption limit cadmium mobility during metabolic activity ofGeobacter sulfurreducens. Environ Sci: Process Impacts 22 (9), 1877–1887.
[51] Tu, C., He, T., Liu, C., Lu, X., Lang, Y., 2011. Accumulation of trace elements in agricultural topsoil under different geological background. Plant Soil 349 (1–2), 241–251.
[52] Uddin, M.K., 2017. A review on the adsorption of heavy metals by clay minerals, with special focus on the past decade. Chem Eng J 308, 438–462.
[53] Wang, J., Wang, P., Gu, Y., Kopittke, P.M., Zhao, F., Wang, P., 2019. Iron–manganese (Oxyhydro)oxides, rather than oxidation of sulfides, determine mobilization of Cd during soil drainage in paddy soil systems. Environ Sci Technol 53 (5), 2500–2508.
[54] Weber, J., Tyszka, R., Kocowicz, A., Szadorski, J., Debicka, M., Jamroz, E., 2012. Mineralogical composition of the clay fraction of soils derived from granitoids of the Sudetes and Fore-Sudetic Block, southwest Poland. Eur J Soil Sci 63 (5), 762–772.
[55] Wen, Li, Yang, Zhang, Ji, 2020. Enrichment and source identification of Cd and other heavy metals in soils with high geochemical background in the karst region, Southwestern China. Chemosphere 245, 125620.
[56] Wen, Y., Li, W., Yang, Z., Zhuo, X., Guan, D., Song, Y., et al., 2020. Evaluation of various approaches to predict cadmium bioavailability to rice grown in soils with high geochemical background in the karst region, Southwestern China. Environ Pollut 258, 113645.
[57] Xia, X., Ji, J., Zhang, C., Yang, Z., Shi, H., 2022. Carbonate bedrock control of soil Cd background in Southwestern China: Its extent and influencing factors based on spatial analysis. Chemosphere 290, 133390.
[58] Xia, X., Ji, J., Yang, Z., Han, H., Huang, C., Li, Y., et al., 2020. Cadmium risk in the soil-plant system caused by weathering of carbonate bedrock. Chemosphere 254, 126799.
[59] Yan, M., Li, W., Zhao, J., Yin, W., Li, P., Fang, Z., et al., 2022. Enhanced cadmium immobilization by sulfate-mediated microbial zero-valent iron corrosion. J Environ Manag 301, 113894.
[60] Yang, Q., Yang, Z., Zhang, Q., Liu, X., Zhuo, X., Wu, T., et al., 2021. Ecological risk assessment of Cd and other heavy metals in soil-rice system in the karst areas with high geochemical background of Guangxi, China. Sci China Earth Sci 64 (7), 1126–1139.
[61] Yu, H.-Y., Li, F.-B., Liu, C.-S., Huang, W., Liu, T.-X., Yu, W.-M., 2016. Iron redox cycling coupled to transformation and immobilization of heavy metals: implications for paddy rice safety in the red soil of South China. Adv Agron 279–317.
[62] Yue, Z., Li, Q., Li, C., Chen, T., Wang, J., 2015. Component analysis and heavy metal adsorption ability of extracellular polymeric substances (EPS) from sulfate reducing bacteria. Bioresour Technol 194, 399–402.
[63] Zhang, H., Li, H., Li, M., Luo, D., Chen, Y., Chen, D., et al., 2018. Immobilizing metal-resistant sulfate-reducing bacteria for cadmium removal from aqueous solutions. Pol J Environ Stud 27 (6), 2851–2859.
[64] Zhang, K., Yang, Y., Chi, W., Chen, G., Du, Y., Hu, S., et al., 2023. Chromium transformation driven by iron redox cycling in basalt-derived paddy soil with high geological background values. J Environ Sci 125, 470–479.
[65] Zhao, Q., Li, X., Wang, Y., Cheng, Y., Fan, W., 2023. Long-term bioremediation of cadmium contaminated sediment using sulfate reducing bacteria: Perspective on different depths of the sediment profile. Chem Eng J 451, 138697.